Colloidal CdSe/Cu_3P/CdSe Nanocrystal Heterostructures and Their Evolution upon Thermal Annealing

Luca De Trizio, Francesco De Donato, Alberto Casu, Alessandro Genovese, Andrea Falqui,* Mauro Povia, and Liberato Manna*

Department of Nanochemistry, Istituto Italiano di Tecnologia, Via Morego 30, 16163 Genova, Italy

ABSTRACT We report the synthesis of colloidal CdSe/Cu_3P/CdSe nanocrystal heterostructures grown from hexagonal Cu_3P platelets as templates. One type of heterostructure was a sort of "coral", formed by vertical pillars of CdSe grown preferentially on both basal facets of a Cu_3P platelet and at its edges. Another type of heterostructure had a "sandwich" type of architecture, formed by two thick, epitaxial CdSe layers encasing the original Cu_3P platelet. When the sandwiches were annealed under vacuum up to 450 °C, sublimation of P and Cd species with concomitant interdiffusion of Cu and Se species was observed by *in situ* HR- and EFTEM analyses. These processes transformed the starting sandwiches into Cu_2Se nanoplatelets. Under the same conditions, both the pristine (uncoated) Cu_3P platelets and a control sample made of isolated CdSe nanocrystals were stable. Therefore, the thermal instability of the sandwiches under vacuum might be explained by the diffusion of Cu species from Cu_3P cores into CdSe domains, which triggered sublimation of Cd, as well as out-diffusion of P species and their partial sublimation, together with the overall transformation of the sandwiches into Cu_2Se nanocrystals. A similar fate was followed by the coral-like structures. These CdSe/Cu_3P/CdSe nanocrystals are therefore an example of a nanostructure that is thermally unstable, despite its separate components showing to be stable under the same conditions.

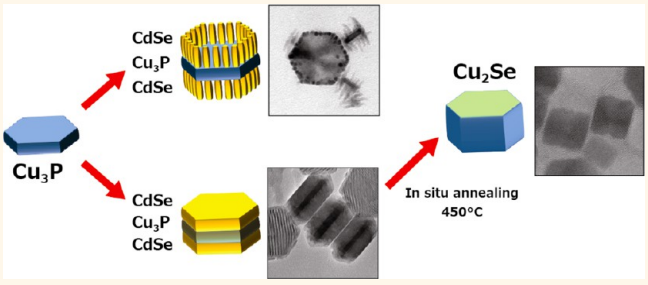

KEYWORDS: nanocrystals · heterostructures · annealing · cation exchange · doping

The synthesis of colloidal nanocrystals (NCs) is rapidly evolving toward the creation of elaborate structures. Examples in this direction are NC heterostructures; that is, nanoparticles in which various sections of different materials and/or crystal phases are connected together.[1−27] NC heterostructures are mostly fabricated by a seeded growth approach that consists of using preformed NCs, of a given material, as "seeds" onto which domains of other materials are grown. Another common way to synthesize nanoheterostructures is to start from preformed NCs as templates, in which specific crystal domains of the original structure are converted into different materials through partial cation exchange.[1,2,12,24,28]

Another possible way of realizing complex NC structures is by combining colloidal synthesis of heterostructures with postsynthetic thermal heating.[7,16] In the case of metal−semiconductor heterostructures, this procedure has made it possible to fabricate peculiar NCs, for example, Au−CdSe nanodumbbells consisting of Au and CdSe domains connected together *via* epitaxial interfaces, which cannot be achieved directly in the solution phase.[7] Thermal annealing in conjunction with electron irradiation can also be exploited to create new nanostructures *in situ*, although this field is still in its infancy.[22] One key point of NC heterostructures is that the relative thermal or irradiation stability/reactivity of a certain material domain in the heterostructure can be much different from that of the same domain if it were the only constituent of the NC. This is due to its proximity to domains of other materials that can elicit concomitant processes such as diffusion of chemicals, alloying, charge transfer and others. For example, while separate CdS and Au NCs are both relatively stable to electron irradiation, CdS−Au NC heterostructures rapidly

* Address correspondence to andrea.falqui@iit.it, liberato.manna@iit.it.

Received for review December 29, 2012 and accepted April 3, 2013.

Published online April 04, 2013
10.1021/nn3060219

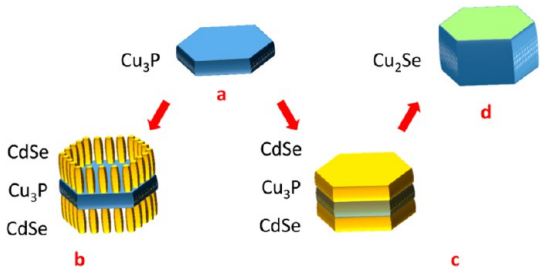

Scheme 1. Formation of various CdSe/Cu_3P/CdSe heterostructures and Cu_2Se nanoplatelets by combining chemical synthesis followed by thermal annealing: (a) Cu_3P platelets; (b) nanocorals, that is, Cu_3P nanoplatelets decorated with CdSe pillars at the edges of their basal facets; (c) CdSe/Cu_3P/CdSe sandwiches; (d) Cu_2Se NCs obtained from the sandwiches by thermal annealing

decompose under the same conditions and form AuS(core)/Cd(shell) NCs.[22]

We report here the synthesis of various nanostructures by combining colloidal synthesis with post-synthetic thermal annealing. Starting from hexagonal Cu_3P platelets (Scheme 1a), we could prepare structures resembling corals, in which vertical pillars of CdSe were grown preferentially at the edges of the Cu_3P platelets, on both basal facets (Scheme 1b). With different concentrations of surfactants, and working at higher temperatures, we could instead grow sandwich-shaped nanoparticles consisting of one top and one bottom layer of CdSe encasing each original Cu_3P platelet (Scheme 1c). Upon thermal annealing, these sandwich-like nanostructures were transformed into in Cu_2Se NCs (Scheme 1d). Under the same conditions, the pristine, uncoated Cu_3P platelets were stable[9,29] and even CdSe NCs, synthesized by standard methods, did not undergo noticeable compositional changes under the same annealing process (see Figure S5).[29] Therefore, these CdSe/Cu_3P/CdSe sandwiches are an example of thermally unstable nanostructures, despite being built by combining subunits that separately would be otherwise stable. In the present case, the instability appeared to be driven by high diffusion rate of Cu into the nearest neighbor phases. This diffusion seemed to trigger not only the sublimation of Cd, which was replaced by Cu, but also the out-diffusion of P and its partial sublimation, as we already observed in our previous work[9] on Cu_3P/Cu Janus-like particles. The final effect was therefore a conversion of the original sandwiches to Cu_2Se NCs. A similar fate was followed by the coral-like structures, although it required slightly higher temperatures.

Apart from synthetic considerations discussed here, the results of subjecting NCs to conditions such as annealing or irradiation can have important technological implications. For example, NCs that would degrade quickly under oxygen/moisture or under various processing conditions could instead be generated *in situ* in a protected environment at the last steps of a device fabrication process. Also, similar procedures may be exploited to achieve NCs with new phase compositions that would be otherwise problematical to fabricate in the solution phase. Finally, as increasingly more applications are envisaged that are based on nanoscale materials, it is clearly important to make assessments on the long time stability of such materials. Thermal annealing can be a convenient method for assessing such stability.

RESULTS AND DISCUSSION

Synthesis of CdSe/Cu_3P/CdSe Nanocorals and Sandwich-like Nanostructures. In all the syntheses reported in this work, CdSe was grown on presynthesized Cu_3P platelets, in a mixture of trioctylphosphine oxide and a combination of alkylphosphonic acids, namely, hexylphosphonic acid (HPA) and octadecylphosphonic acid (ODPA), in a temperature range between 300 and 380 °C. In all these syntheses, the exclusive growth of CdSe on top of the Cu_3P nanoplatelets, without side nucleation of CdSe nanoparticles in solution, was possible by the addition of small amounts of HCl. This is similar to what shown recently by us on seeded grown branched CdSe/CdS NCs, in that case using $CdCl_2$ in small concentrations in addition to CdO as Cd precursor.[30] Figure 1 reports transmission electron microscopy (TEM) images of initial Cu_3P platelets (Figure 1a) and of corals grown under different reaction conditions (Figure 1b,c). For the syntheses carried out at 300 °C (Figure 1b), it is clear that many thin CdSe pillars grew preferentially at the edges of the basal facets of the Cu_3P platelets. This selectivity was most likely driven by the higher reactivity of the edges of the platelets, where more active sites would favor nucleation of CdSe. Also, the vast majority of CdSe pillars grew vertically with respect to the Cu_3P substrate, an indication that the initial platelets provided a directionality that is likely driven by an epitaxial relationship between the basal facet of Cu_3P and one (or both) polar facet(s) of CdSe perpendicular to the [001] elongation direction of the pillars. Both CdSe and Cu_3P have indeed hexagonal symmetry and many sets of lattice planes of the two phases are characterized by similar spacing. At reaction temperatures higher than 300 °C, different heterostructures were obtained (Figure 1c). For example, at 340 °C, in addition to observing growth of CdSe pillars at the edges (which were thicker in this case), other pillars were noticed also in the central region of the basal facets of the platelets (see inset of Figure 1c). In addition, a CdSe layer covered each platelet, as evidenced from the Moiré pattern[31] of the nanoparticles imaged under TEM when laying flat with respect to the substrate.

Sandwich-like heterostructures were formed when increasing the amount of phosphonic acids with respect to that of Cu_3P seeds (Figures 2 and 3a) and performing the synthesis at 380 °C. From various

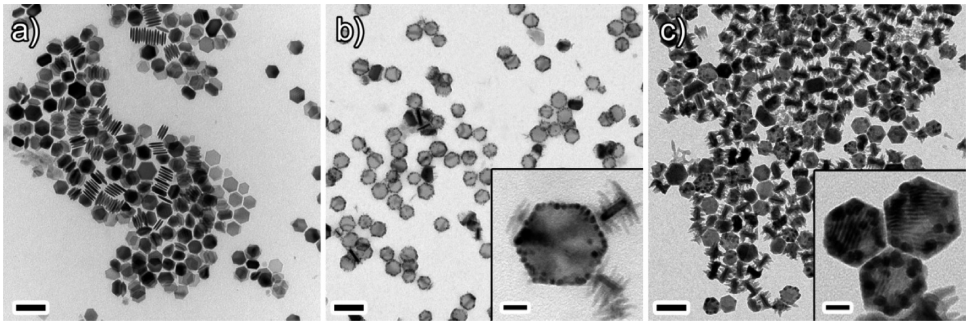

Figure 1. TEM images of (a) initial Cu_3P platelets; (b) nanocorals grown at 300 °C (inset shows a top view of a large coral and side views of smaller corals); (c) nanocorals grown at 340 °C. Here, in the inset, a magnified view of a group of corals is shown, where it is also possible to see the Moiré interference pattern on the platelets. The scale bar is 100 nm in the images and 20 nm in the insets. Both CdSe and Cu_3P have hexagonal structures.

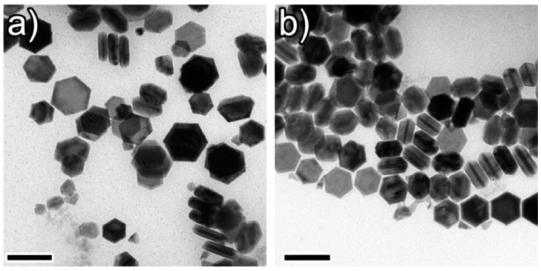

Figure 2. TEM images of CdSe/Cu_3P/CdSe sandwiches grown at 380 °C after (a) 1 min and (b) 8 min. The scale bar is 100 nm in both images.

experiments, we could infer that, first, the presence of HPA promoted the formation of elongated CdSe structures (like the pillars discussed above) on top of the Cu_3P platelets. Instead, when using a higher concentration of ODPA with respect to HPA, a layered growth was favored. We observed indeed that sandwich-like nanostructures were formed even without adding any HPA (see Figure S1a).[29] The thickness of the CdSe layers on the top and on the bottom of the Cu_3P platelets could be increased by varying the reaction time from 1 to 8 min at 380 °C (Figure 2). Sandwiches could also be synthesized at lower temperatures, but with much less control over the thickness of the CdSe layers (see also figure S1b).[29] These experiments suggested that the chemical passivation provided by phosphonic acids governed the heteronucleation of CdSe on Cu_3P, although a detailed understanding of the exact mechanism underlying the growth of the various CdSe/Cu_3P morphologies would require further investigations.

Structural Analysis of the Sandwiches. High-resolution TEM (HRTEM) analysis of the sandwiches indicated phase stacking along the [0001] directions of both CdSe (space group $P6_3mc$, JCPDS card 77-2307) and Cu_3P (space group $P6_3cm$, JCPDS card 71-2261). The double CdSe/Cu_3P/CdSe interface was clearly identified due to the difference of electron absorption between the two phases (Figure 3a). Scanning TEM energy dispersive X-ray (STEM-EDX) line profiling

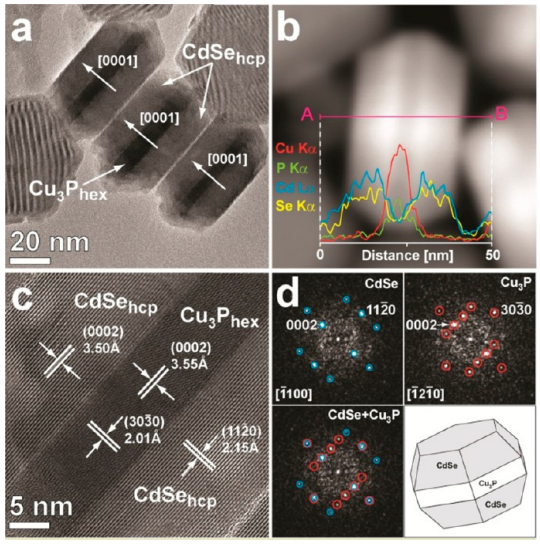

Figure 3. Side-view of CdSe/Cu_3P/CdSe sandwiches. (a) HRTEM image showing the [0001] stacking of the two phases characterized by a different electron contrast; (b) HAADF STEM image and EDX line profile (marked by A and B labels) with Cu Kα, P Kα, Cd Lα and Se Kα signals across a single NC; (c) high magnification HRTEM image of the epitaxial interfaces in a single sandwich. The main (0002) and (11$\bar{2}$0) lattice planes for the CdSe domains and the (0002) and (30$\bar{3}$0) planes for the Cu_3P domains are displayed; (d) FFT patterns of CdSe in blue ([$\bar{1}$100] zone axis) and Cu_3P in red ([$\bar{1}$2$\bar{1}$0] zone axis) showing their lattice similarities (CdSe + Cu_3P FFT pattern); the sketch at the bottom right displays the whole habit of the heterostructure.

displayed the Cu, P, Cd and Se elemental distribution across the crystals (Figure 3b), with a weaker signal of Cd and Se detected in the central region corresponding to Cu_3P platelets and due to X-ray fluorescence coming from the two CdSe external domains. Besides, HRTEM revealed a "twin" epitaxial relationship governing the growth of the CdSe/Cu_3P/CdSe sandwiches (Figure 3c). The two CdSe/Cu_3P interfaces were mutually aligned according to the following symmetry relationships:

$$\text{CdSe}(0002)//\text{Cu}_3\text{P}(0002)$$
$$\text{CdSe}[11\bar{2}0]//\text{Cu}_3\text{P}[30\bar{3}0]$$

where the first term represents the interface alignment and the second one the vector alignment. Along the CdSe(0002)/Cu_3P(0002) interface, it was then possible to calculate the actual lattice mismatch (m), defined as the absolute difference between two lattice spacings (d_1 and d_2) along a certain direction, relative to the average of the lattice spacings:

$$m = 2 \times |d_1 - d_2|/(d_1 + d_2)$$

In particular, the lattice mismatches can be described by considering that one unit cell of CdSe along the directions [0002], [11$\bar{2}$0] and [$\bar{1}$100], fits into one unit cell of Cu_3P along the directions [0002], [30$\bar{3}$0] and [$\bar{1}$2$\bar{1}$0], respectively (Table 1). The Fourier analysis of the HRTEM images of well oriented heterostructures was performed by means of filtered 2D-Fast Fourier Transform (FFT) and proved the alignment of the epitaxial-related domains. Figure 3d displays the FFT patterns of CdSe shells, Cu_3P core and the whole habit of these heterostructures. It is noticeable that the [$\bar{1}$100] zone axis projection of the CdSe domains is collinear to the [$\bar{1}$2$\bar{1}$0] zone axis projection of the Cu_3P platelet, with only a slight shift between the 11$\bar{2}$0 spots of CdSe and 30$\bar{3}$0 of Cu_3P, due to small differences between the respective d-spacing. As expected, plan-view HRTEM observations of the sandwiches revealed then the presence of translational Moiré fringes (Figure 3a) generated by the interference of CdSe (11$\bar{2}$0) and Cu_3P (30$\bar{3}$0) lattice sets which exhibited closed d-spacing with values of 2.15 and 2.01 Å, respectively.[29]

TABLE 1. Lattice Mismatches at the CdSe(0002)/Cu_3P(0002) Interface

Commensurate Lattice Mismatches m	
CdSe/Cu_3P	M
[0002]//[0002]	1.4%
[11$\bar{2}$0]//[30$\bar{3}$0]	6.2%
[$\bar{1}$100]//[$\bar{1}$210]	6.6%

Annealing Experiments. Annealing experiments were performed by heating the samples both *in situ*, *i.e.*, in the TEM, on NCs deposited on Ni and Cu grids, and *ex situ*, that is, in a heating chamber under vacuum, on NCs films deposited on silicon substrates. We discuss first the results of the *in situ* annealing experiments, which were performed using a TEM sample holder capable to reach temperatures up to of 800 °C. These are shown in Figure 4, which reports a sequence of HRTEM images of a single CdSe/Cu_3P/CdSe heterostructure from room temperature (Figure 4a) up to 400 °C (Figure 4b,c). Upon heating to 350 °C, in most sandwiches the CdSe domains of the original heterostructures (Figure 4a) showed a transition to a lattice compatible with fcc Cu_2Se, while the central region was still compatible with Cu_3P (Figure 4b) and the interface between CdSe and Cu_3P was blurry. It is interesting to note that, while the reaction temperature of 380 °C at which the colloidal synthesis was made did not cause any phase modification of the formed heterostructures, annealing experiments, carried under high vacuum, did show structural evolution in the sandwiches already at 350 °C. This point will be discussed later in detail. Further heating to 400 °C determined the complete transformation of each original heterostructure into a NC that was thoroughly characterized by a fcc lattice, with d-spacings compatible with those of fcc Cu_2Se (Figure 4c).

Also, energy filtered TEM (EFTEM) maps of Cu, Cd and P were acquired on an area of the grid containing several sandwiches during the observed transition (Figure 5). These maps revealed a migration of all the elements starting from 350 °C up to 450 °C. Such migration resulted in the extrusion of the P and Cd atoms from the heterostructures, while the Cu atoms were distributed all over the NCs.

We observed an incipient destabilization process at 400 °C, followed by a partial "dissolution" of nanoparticles (NCs). This effect was more evident and rapid

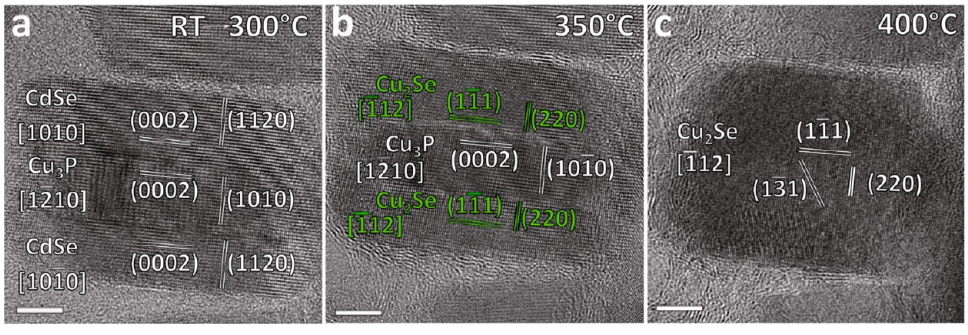

Figure 4. *In situ* annealing experiments on a single CdSe/Cu_3P/CdSe heterostructure monitored by HRTEM using an ultrathin Cu grid. (a) The NC at room temperature (the structure was stable at 300 °C). (b) HRTEM acquired at 350 °C, where the CdSe domains were already transformed to Cu_2Se and this latter phase is first observed. c) HRTEM acquired at 400 °C, where the sole Cu_2Se phase is observed along the [$\bar{1}$12] zone axis, with fcc crystal structure exhibiting (1$\bar{1}$1) and (220) lattice sets with measured d-spacings of 3.37 and 2.06 Å, respectively. All the scale bars reported correspond to a length of 5 nm.

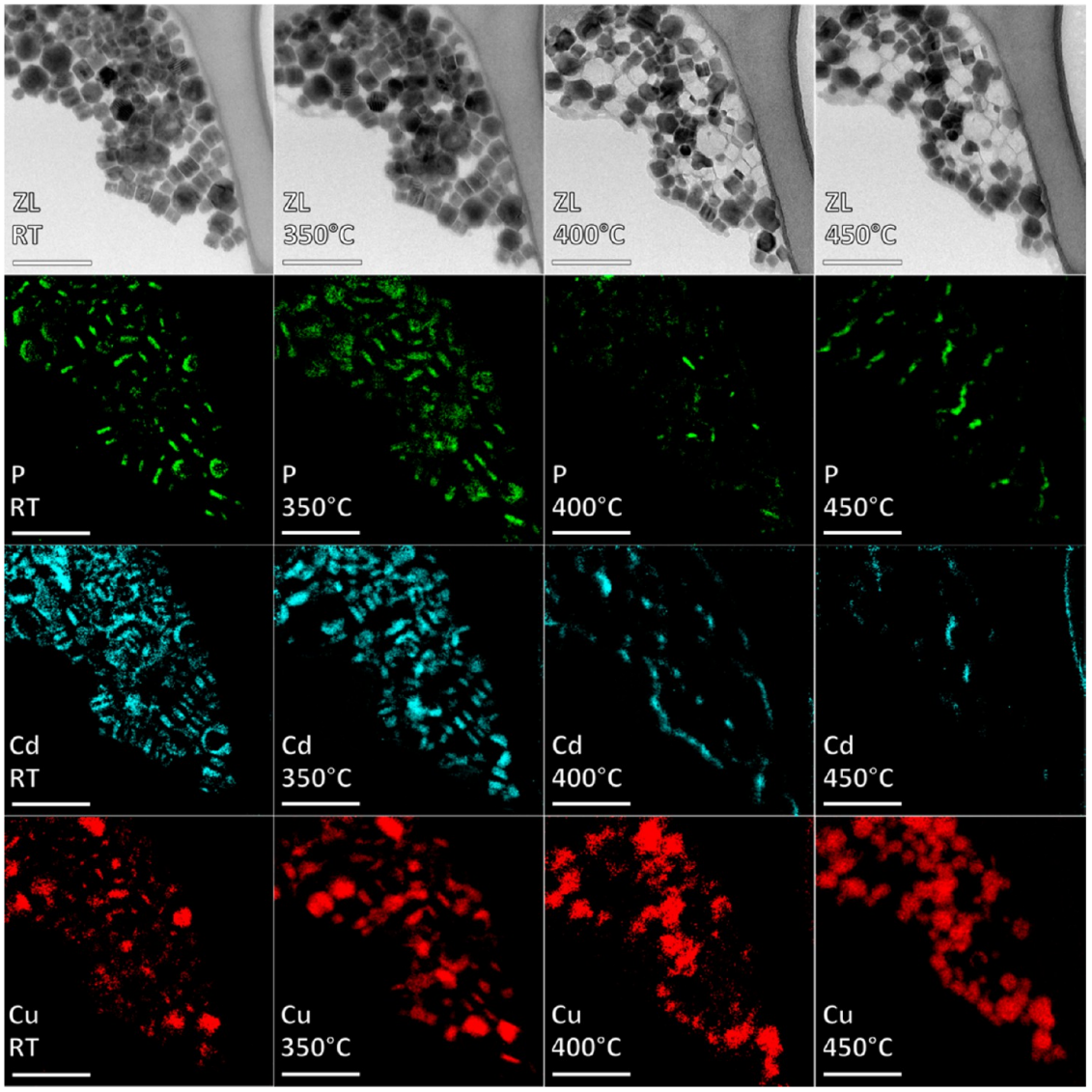

Figure 5. Elastic filtered image (ZL) and EFTEM elemental maps of several sandwiches between room temperature (RT) and 450 °C on an ultrathin Cu grid. Elemental maps were obtained by using the EELS L-edges of P (132 eV, depicted in green), Cd (404 eV, depicted in cyan), and Cu (931 eV, depicted in red), respectively. All the scale bars reported correspond to a length of 100 nm.

when the sample was heated for a few minutes (5−10 min) at a temperature of 450 °C. Under these conditions, some NCs developed alteration/dissolution figures and some of them eventually sublimated altogether. In particular, the EFTEM mapping exhibited a partial rearrangement of the P atoms in the peripheral regions of the sandwiches and the concomitant and complete loss of the Cd atoms between 400° and 450 °C (this could be better observed in Figure 6 on a smaller group of particles), probably due to a thermal sublimation process under the high vacuum conditions of the TEM. The separation between Cu_3P and CdSe domains, initially easily distinguishable from the corresponding zero-loss (ZL) images at RT, became blurry at higher temperatures as a consequence of Cu ions diffusion in the sandwiches, associated to P and Cd loss. Additional EFTEM images, taken during annealing of other samples, confirmed the reproducibility of these observations. The absence of Cd from the annealed NCs was also confirmed by a subsequent STEM-EDX analysis, where no signal from Cd could be found (see Figure S3 of the Supporting Information). This process was clearly visible when monitoring the annealing evolution of the sandwiches in side-view.

On the light of EFTEM data and spatially resolved EDX analysis, we can better explain the structural transformation of sandwich NCs shown in Figure 4 assessing that the loss of Cd atoms is associated with the appearance of Cu_2Se domains. Moreover, such domains exhibited a "mimetic" growth in sub-solidus conditions, *i.e.*, they maintained the original orientation of the starting hexagonal CdSe phase considering the closed packed arrangement of Se atoms in the two structures,

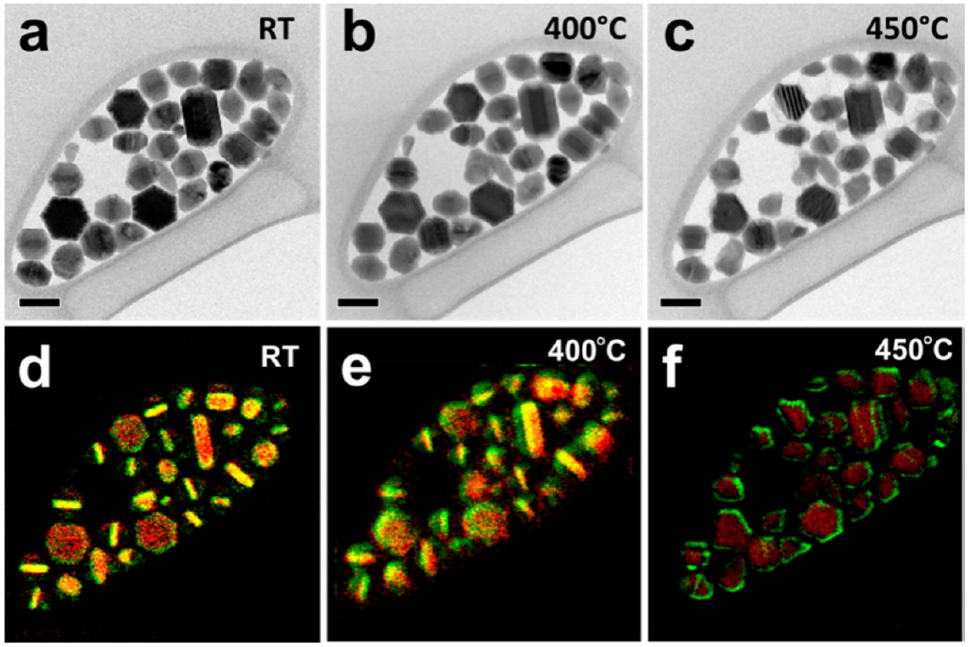

Figure 6. Elastic filtered images, zero loss (a−c), and the corresponding EFTEM elemental maps (d−f) of several NCs observed at room temperature (RT), 400 and 450 °C. Elemental maps were obtained by using the EELS L-edges of P (132 eV, depicted in green,) and Cu (931 eV, depicted in red), respectively. The ZL image collected at 450 °C shows clearly sublimation morphologies. All the scale bars reported correspond to a length of 50 nm.

namely, fcc for Cu_2Se and hcp for CdSe (compare panel a with panel c of Figure 4).

In parallel to such diffusion processes which transformed the original sandwiches to Cu_2Se NCs, several sandwiches instead did sublimate entirely. This can be seen by comparing the sequence of zero loss images (ZL) of Figure 5. The reason for this is still unclear, but most likely it was driven by the diffusion of atomic species among neighboring nanocrystals when the interparticle distance was short enough. It appeared therefore that annealing under high vacuum, which triggered the interdiffusion of some atomic species and the sublimation of others, could set the NC into a potentially unstable configuration. Several *in situ* annealing experiments were run to confirm the observations above (both transformation into Cu_2Se and sublimation). Also, one important remark to make is that, when the initial Cu_3P platelets or even isolated CdSe NCs were subject to the same annealing conditions as for the sandwiches (or even to higher temperature), no morphological, compositional or structural changes were observed (see Figure S4).

Similar annealing experiments were also carried out on nanocorals NCs (results are reported in the Supporting Information section). The EFTEM maps acquired at increasing temperatures confirmed also for these CdSe/Cu_3P/CdSe heterostructures their thermal instability. In this case, however, the destabilization and dissolution process was observed on the NCs at a temperature of 500−550 °C. These values are slightly higher than the corresponding sandwich-like nanostructures. The cause could be ascribed to the presence of a residual organic shell covering the NCs that interfered with the ion diffusion and sublimation processes (Figure S5).

To ensure that the observed chemical transformations occurred in the whole sample of sandwich-like NCs and that they were not due to a combined effect of annealing and electron irradiation, we carried out *ex situ* annealing experiments on films of sandwiches deposited on a silicon substrate. The annealing was done in a vacuum chamber ($\sim 10^{-8}$ Torr) in conditions as similar as possible to the ones used in the TEM. XRD patterns of the sample before and after annealing were recorded at room temperature under air and are reported in Figure 7. The XRD pattern of the initial sandwiches was dominated by diffraction peaks of CdSe domains, with small contributions from Cu_3P domains. After annealing, the XRD pattern exhibited new and sharp diffraction peaks that could be indexed with the α phase of Cu_2Se (some of the small peaks present in the patterns after annealing could be due to residuals of the starting NCs or to small fractions of unidentified compounds formed as a consequence of the annealing). The β-Cu_2Se phase, with cubic lattice, is what we observed in the *in situ* annealing experiments in the TEM. Indeed, the α-Cu_2Se polymorph is the low-temperature phase that evolves to the β-Cu_2Se polymorph above 130 °C.[32,33]

The XRD analysis on a film of annealed NCs confirmed that the transformation from the CdSe/Cu_3P/CdSe heterostructures to Cu_2Se did not require electron irradiation. As discussed earlier, this transformation appears to be triggered by both the ease of diffusion of Cu into CdSe and the sublimation of Cd

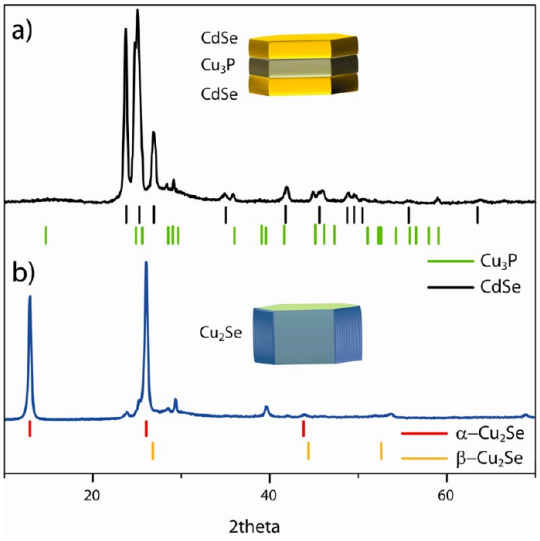

Figure 7. (a) XRD patterns of a film of initial CdSe/Cu_3P/CdSe sandwiches, with corresponding bulk positions for the CdSe (JCPDS card 00-002-0330) and Cu_3P (JCPDS card 03-065-3628) phases. (b) XRD pattern from the same film, after annealing at 400 °C for 45 min, along with bulk positions for the monoclinic α-Cu_2Se[33] and cubic β-Cu_2Se (JCPDS card 00-004-0839) phases. Some of the small peaks present in the patterns after annealing could be due to residuals of the starting NCs or to small fractions of unidentified compounds formed as a consequence of the annealing.

(and partially of P) under the annealing conditions. Cu is a well-known dopant in many II–VI semiconductors, and studies of Cu–CdS and Cu–CdSe interfaces evidenced the formation of a thick interfacial layer in which dissociated Cd and Cu–chalcogen alloy were present.[34] The fact that CdSe/Cu_3P/CdSe sandwiches in solution were stable at 380 °C, while the same NCs on a substrate were unstable at those temperatures under vacuum, is noteworthy. In the annealing experiments on samples deposited on substrates, the ultrahigh vacuum conditions, both in the *in situ* and in the *ex situ* experiments, certainly favored the sublimation of Cd. On the other hand, when the sandwiches were synthesized in solution, Cd ions/atoms were less prone to leave the CdSe lattice in order to make room for the Cu ions/atoms coming from the Cu_3P lattice. This was most likely due to the presence of a considerable amount of unreacted Cd species during the synthesis, which made the ejection of Cd from the sandwiches unfavorable. Another reason for the stability of the heterostructures when heated in solution might be due to the abundant presence of ligands that allow for the protection of the NCs. In fact, the same cannot happen when annealing the nanostructures on substrates, where the combined effect of heating and vacuum can lead to ligand desorption.[35] Annealing in solution can instead lead to ligand exchange.[36]

CONCLUSIONS

We have reported in this work the synthesis of various types of CdSe/Cu_3P/CdSe nanoheterostructures and we have studied their thermal evolution. In the case of sandwiches, these could be transformed to Cu_2Se platelets by annealing. One important conclusion from this work is that thermal annealing of nanoheterostructures can be exploited to create new types of nanostructures. Also, Cu_2Se is a potentially interesting material for its plasmonic properties in the near-infrared, provided that a fraction of its Cu atoms are extracted to yield a compound with substoichiometric composition.[37,38] Therefore, one further development in this direction could be that of creating plasmonic micro- and nanostructures "on demand", for example, by annealing with a laser individual or groups of CdSe/Cu_3P/CdSe NCs deposited on a substrate.

EXPERIMENTAL SECTION

Chemicals. Copper chloride (CuCl, 99.999%), elemental selenium (Se, 99.99%), trioctylphosphine oxide (TOPO, 99%) and tri-*n*-octylphosphine (TOP, min. 97%) were purchased from Strem Chemicals. Octadecylphosphonic acid (ODPA) and hexylphosphonic acid (HPA) were purchased from Polycarbon Industries. Cadmium oxide (CdO, 99.5%), 1-octadecene (ODE 90%), hydrochloridric acid (HCl, 37%) and the various anhydrous solvents were purchased from Sigma-Aldrich.

Synthesis Procedures. The initial Cu_3P platelets were synthesized according to a procedure described by us recently, with minor modifications (see Supporting Information for additional details).[9]

Synthesis of CdSe/Cu_3P/CdSe Nanocorals. Nanocorals, that is, Cu_3P nanoplatelets decorated with CdSe pillars, were generally synthesized in a temperature range between 300 and 340 °C. In a typical synthesis of "nanocorals", 3 g of TOPO was mixed with 30 mg of CdO, 40 mg of HPA, 145 mg of ODPA, and 20 μL of HCl solution (obtained adding 50 μL of 37% HCl to 10 mL of Milli-Q grade H_2O) in a three-neck flask. The mixture was heated under vacuum to 150 °C and degassed at this temperature for 2 h. Then, under nitrogen flux, 1,5 mL of TOP was added and the temperature was raised to 300 °C. At this point, a solution of Cu_3P NCs dissolved in 0.5 mL of ODE (the concentration of Cu^+ was calculated to be 12 mM by inductively coupled plasma atomic emission spectroscopy (ICP-AES)) was mixed with 0.3 mL of a TOP-Se solution (the latter prepared by dissolving Se in TOP, 12 mg/mL of selenium) and the resulting solution was then injected into the flask. The reaction was run for 8 min at 300 °C, after which the flask was cooled to room temperature. The particles were precipitated with addition of methanol and then washed three times by dispersion in toluene followed by precipitation *via* addition of methanol (the amount of precursors and synthetic parameters used in the syntheses reported in the text are also summarized in Table S1).

Synthesis of CdSe/Cu_3P/CdSe Sandwich-like Nanostructures. These were synthesized under conditions different from those of the nanocorals, most notably at temperatures around 380 °C, but also working with slightly different ratios of reactants to optimize the yield in sandwiches. As an example, CdSe/Cu_3P/CdSe sandwiches were prepared by following the same synthetic process described above, but using higher loadings of HPA and ODPA (50 and 181 mg, respectively) and by running the synthesis at 380 °C instead of 300 °C. Also, the thickness of the CdSe layers could be tuned by varying the synthesis time. Typical times ranged from 1 to 8 min (the amount of precursors

and synthetic parameters used in the syntheses reported in the text are also summarized in Table S1).

Transmission Electron Microscopy (TEM), Scanning TEM Analysis, and *in Situ* Thermal Annealing. High Resolution TEM (HRTEM), Scanning TEM (STEM) in High Angular Annular Dark Field (HAADF) geometry, and Energy Filtered TEM (EFTEM) imaging were performed with a JEOL JEM-2200FS microscope, equipped with a field emission gun working at an accelerating voltage of 200 kV, a CEOS spherical aberration corrector of the objective lens allowing to get a spatial resolution of 1 Å, and an in column Omega energy filter. Single particle chemical composition was determined for several particles by Energy Dispersive X-ray Spectroscopy (EDS) analysis performed in STEM mode, with a JED-2300 Si(Li) detector and an electron probe size of 0.7 nm. EFTEM images were acquired using a contrast aperture of about 10 mrad to reduce aberrations (mostly chromatic) and filtering the Zero Loss (ZL) peak using an energy slit of 10 eV, and the electron energy loss (EEL) edges of P (132 eV), and Cd (404 eV) using an energy slit of 20 eV, and of Cu (931 eV), in the latter case with the width of the energy slit equal to 50 eV. The *in situ* thermal annealing experiments were performed using a JEOL EM-21130 single tilt heating holder capable to reach temperatures up to of 800 °C.

X-ray Powder Diffraction (XRD). XRD measurements were performed on a Rigaku SmartLab X-ray diffractometer operating at 40 kV and 150 mA. The diffractometer was equipped with Cu source and a Gobel mirror in order to have a parallel beam and it was used in 2-theta/omega scan geometry for the acquisition of the data. Specimens for XRD measurements were prepared in the glovebox by dropping a concentrated NCs solution onto a zero-background silicon substrate. For experiments on thermally annealed samples, the silicon substrate with the NCs film on top was annealed at 400 °C under vacuum ($\sim 10^{-8}$ Torr) for 45 min, after which the sample was cooled to room temperature and its XRD pattern was recorded at room temperature in air.

Conflict of Interest: The authors declare no competing financial interest.

Supporting Information Available: Additional data on: TEM analysis; XRD analysis. This material is available free of charge *via* the Internet at http://pubs.acs.org."

Acknowledgment. The authors acknowledge financial support from European Union through the FP7 starting ERC grant NANO-ARCH (contract no. 240111). We thank Marijn van Huis and Anil Yalcin for many useful discussions.

REFERENCES AND NOTES

1. Costi, R.; Saunders, A. E.; Banin, U. Colloidal Hybrid Nanostructures: A New Type of Functional Materials. *Angew. Chem., Int. Ed.* **2010**, *49*, 4878–4897.
2. Robinson, R. D.; Sadtler, B.; Demchenko, D. O.; Erdonmez, C. K.; Wang, L.-W.; Alivisatos, A. P. Spontaneous Superlattice Formation in Nanorods through Partial Cation Exchange. *Science* **2007**, *317*, 355–358.
3. Mokari, T. Synthesis and Characterization of Hybrid Nanostructures. *Nano Rev.* **2011**, *2*, 5983.
4. Vinokurov, K.; Macdonald, J. E.; Banin, U. Structures and Mechanisms in the Growth of Hybrid Ru−Cu_2S Nanoparticles: From Cages to Nanonets. *Chem. Mater.* **2012**, *24*, 1822–1827.
5. Shen, S.; Zhang, Y.; Liu, Y.; Peng, L.; Chen, X.; Wang, Q. Manganese-Doped Ag_2S-ZnS Heteronanostructures. *Chem. Mater.* **2012**, *24*, 2407–2413.
6. Wu, K.; Zhu, H.; Liu, Z.; Rodríguez-Córdoba, W.; Lian, T. Ultrafast Charge Separation and Long-Lived Charge Separated State in Photocatalytic CdS−Pt Nanorod Heterostructures. *J. Am. Chem. Soc.* **2012**, *134*, 10337–10340.
7. Figuerola, A.; Huis, M. v.; Zanella, M.; Genovese, A.; Marras, S.; Falqui, A.; Zandbergen, H. W.; Cingolani, R.; Manna, L. Epitaxial CdSe-Au Nanocrystal Heterostructures by Thermal Annealing. *Nano Lett.* **2010**, *10*, 3028–3036.
8. Macdonald, J. E.; Bar Sadan, M.; Houben, L.; Popov, I.; Banin, U. Hybrid Nanoscale Inorganic Cages. *Nat. Mater.* **2010**, *9*, 810–815.
9. De Trizio, L.; Figuerola, A.; Manna, L.; Genovese, A.; George, C.; Brescia, R.; Saghi, Z.; Simonutti, R.; Van Huis, M.; Falqui, A. Size-Tunable, Hexagonal Plate-like Cu_3P and Janus-like Cu−Cu_3P Nanocrystals. *ACS Nano* **2012**, *6*, 32–41.
10. Amirav, L.; Alivisatos, A. P. Photocatalytic Hydrogen Production with Tunable Nanorod Heterostructures. *J. Phys. Chem. Lett.* **2010**, *1*, 1051–1054.
11. Shemesh, Y.; Macdonald, J. E.; Menagen, G.; Banin, U. Synthesis and Photocatalytic Properties of a Family of CdS-Pd_X Hybrid Nanoparticles. *Angew. Chem., Int. Ed.* **2011**, *50*, 1185–1189.
12. Rivest, J. B.; Swisher, S. L.; Fong, L.-K.; Zheng, H.; Alivisatos, A. P. Assembled Monolayer Nanorod Heterojunctions. *ACS Nano* **2011**, *5*, 3811–3816.
13. Sitt, A.; Salant, A.; Menagen, G.; Banin, U. Highly Emissive Nano Rod-in-Rod Heterostructures with Strong Linear Polarization. *Nano Lett.* **2011**, *11*, 2054–2060.
14. Li, P.; Lappas, A.; Lavieville, R.; Zhang, Y.; Krahne, R. CdSe−Au Nanorod Networks Welded by Gold Domains: A Promising Structure for Nano-Optoelectronic Components. *J. Nanopart. Res.* **2012**, *14*, 1–5.
15. Figuerola, A.; Fiore, A.; Di Corato, R.; Falqui, A.; Giannini, C.; Micotti, E.; Lascialfari, A.; Corti, M.; Cingolani, R.; Pellegrino, T.; et al. One-Pot Synthesis and Characterization of Size-Controlled Bimagnetic FePt−Iron Oxide Heterodimer Nanocrystals. *J. Am. Chem. Soc.* **2008**, *130*, 1477–1487.
16. George, C.; Dorfs, D.; Bertoni, G.; Falqui, A.; Genovese, A.; Pellegrino, T.; Roig, A.; Quarta, A.; Comparelli, R.; Curri, M. L.; et al. A Cast-Mold Approach to Iron Oxide and Pt/Iron Oxide Nanocontainers and Nanoparticles with a Reactive Concave Surface. *J. Am. Chem. Soc.* **2011**, *133*, 2205–2217.
17. Yu, H.; Chen, M.; Rice, P. M.; Wang, S. X.; White, R. L.; Sun, S. Dumbbell-like Bifunctional Au−Fe_3O_4 Nanoparticles. *Nano Lett.* **2005**, *5*, 379–382.
18. George, C.; Genovese, A.; Qiao, F.; Korobchevskaya, K.; Comin, A.; Falqui, A.; Marras, S.; Roig, A.; Zhang, Y.; Krahne, R.; et al. Optical and Electrical Properties of Colloidal (Spherical Au)-(Spinel Ferrite Nanorod) Heterostructures. *Nanoscale* **2011**, *3*, 4647–4654.
19. Krylova, G.; Giovanetti, L. J.; Requejo, F. G.; Dimitrijevic, N. M.; Prakapenka, A.; Shevchenko, E. V. Study of Nucleation and Growth Mechanism of the Metallic Nanodumbbells. *J. Am. Chem. Soc.* **2012**, *134*, 4384–4392.
20. Kong, L.; Chen, W.; Ma, D.; Yang, Y.; Liu, S.; Huang, S. Size Control of Au@Cu_2O Octahedra for Excellent Photocatalytic Performance. *J. Mater. Chem.* **2012**, *22*, 719–724.
21. Mokari, T.; Rothenberg, E.; Popov, I.; Costi, R.; Banin, U. Selective Growth of Metal Tips onto Semiconductor Quantum Rods and Tetrapods. *Science* **2004**, *304*, 1787–1790.
22. van Huis, M. A.; Figuerola, A.; Fang, C.; Béché, A.; Zandbergen, H. W.; Manna, L. Chemical Transformation of Au-Tipped CdS Nanorods into AuS/Cd Core/Shell Particles by Electron Beam Irradiation. *Nano Lett.* **2011**, *11*, 4555–4561.
23. Brescia, R.; Miszta, K.; Dorfs, D.; Manna, L.; Bertoni, G. Birth and Growth of Octapod-Shaped Colloidal Nanocrystals Studied by Electron Tomography. *J. Phys. Chem. C* **2011**, *115*, 20128–20133.
24. Miszta, K.; Dorfs, D.; Genovese, A.; Kim, M. R.; Manna, L. Cation Exchange Reactions in Colloidal Branched Nanocrystals. *ACS Nano* **2011**, *5*, 7176–7183.
25. Fiore, A.; Mastria, R.; Lupo, M. G.; Lanzani, G.; Giannini, C.; Carlino, E.; Morello, G.; De Giorgi, M.; Li, Y.; Cingolani, R.; et al. Tetrapod-Shaped Colloidal Nanocrystals of II−VI Semiconductors Prepared by Seeded Growth. *J. Am. Chem. Soc.* **2009**, *131*, 2274–2282.
26. Sun, Y.; Wiley, B.; Li, Z.-Y.; Xia, Y. Synthesis and Optical Properties of Nanorattles and Multiple-Walled Nanoshells/Nanotubes Made of Metal Alloys. *J. Am. Chem. Soc.* **2004**, *126*, 9399–9406.
27. Ithurria, S.; Talapin, D. V. Colloidal Atomic Layer Deposition (c-ALD) using Self-Limiting Reactions at Nanocrystal Surface Coupled to Phase Transfer between Polar and Nonpolar Media. *J. Am. Chem. Soc.* **2012**, *134*, 18585–18590.
28. Sadtler, B.; Demchenko, D. O.; Zheng, H.; Hughes, S. M.; Merkle, M. G.; Dahmen, U.; Wang, L.-W.; Alivisatos, A. P.

Selective Facet Reactivity during Cation Exchange in Cadmium Sulfide Nanorods. *J. Am. Chem. Soc.* **2009**, *131*, 5285–5293.
29. Additional details are reported in the Supporting Information section.
30. Kim, M. R.; Miszta, K.; Povia, M.; Brescia, R.; Christodoulou, S.; Prato, M.; Marras, S.; Manna, L. Influence of Chloride Ions on the Synthesis of Colloidal Branched CdSe/CdS Nanocrystals by Seeded Growth. *ACS Nano* **2012**, *6*, 11088–11096.
31. Williams, B. D.; Carter, C. B. *Transmission Electron Microscopy*; Springer: New York, 2009.
32. Tonejc, A. Phase Diagram and Some Properties of $Cu_{2-x}Se$ (2.01 > 2-x > 1.75). *J. Mater. Sci.* **1980**, *15*, 3090–3094.
33. Gulay, L.; Daszkiewicz, M.; Strok, O.; Pietraszko, A. Crystal Structure of Cu_2Se. *Chem. Mater. Alloy* **2011**, *4*, 200–205.
34. Brucker, C. F.; Brillson, L. J. Reactive Interdiffusion at Metal-CdS and Metal-CdSe Interfaces. *J. Vac. Sci. Technol.* **1981**, *18*, 787–791.
35. Perez-Dieste, V.; Castellini, O. M.; Crain, J. N.; Eriksson, M. A.; Kirakosian, A.; Lin, J.-L.; McChesney, J. L.; Himpsel, F. J.; Black, C. T.; Murray, C. B. Thermal Decomposition of Surfactant Coatings on Co and Ni Nanocrystals. *Appl. Phys. Lett.* **2003**, *83*, 5053–5055.
36. Zhang, S.-Y.; Ye, E.; Liu, S.; Lim, S. H.; Tee, S. Y.; Dong, Z.; Han, M.-Y. Temperature and Chemical Bonding-Directed Self-Assembly of Cobalt Phosphide Nanowires in Reaction Solutions into Vertical and Horizontal Alignments. *Adv. Mater.* **2012**, *24*, 4369–4375.
37. Gorbachev, V. V.; Putilin, I. M. Some Parameters of Band Structure in Copper Selenide and Telluride. *Phys. Status Solidi A* **1973**, *16*, 553–559.
38. Dorfs, D.; Härtling, T.; Miszta, K.; Bigall, N. C.; Kim, M. R.; Genovese, A.; Falqui, A.; Povia, M.; Manna, L. Reversible Tunability of the Near-Infrared Valence Band Plasmon Resonance in $Cu_{2-x}Se$ Nanocrystals. *J. Am. Chem. Soc.* **2011**, *133*, 11175–11180.